Solar Energy Materials & Solar Cells 126 (2014) 83–87

Contents lists available at ScienceDirect

Solar Energy Materials & Solar Cells

journal homepage: www.elsevier.com/locate/solmat

Submonolayer InGaAs/GaAs quantum dot solar cells

Phu Lam [a], Jiang Wu [a,*], Mingchu Tang [a], Qi Jiang [a], Sabina Hatch [a], Richard Beanland [b], James Wilson [c], Rebecca Allison [c], Huiyun Liu [a]

[a] Department of Electronic and Electrical Engineering, University College London, Torrington Place, London WC1E 7JE, UK
[b] Department of Physics, University of Warwick, Coventry CV4 7AL, UK
[c] Defence Science and Technology Laboratory, Portsdown West, Portsdown Hill Road, Fareham Hants PO17 6AD, UK

ARTICLE INFO

Article history:
Received 17 December 2013
Received in revised form
4 February 2014
Accepted 24 March 2014
Available online 15 April 2014

Keywords:
Solar cells
III–V semiconductors
Submonolayer
Quantum dots
Molecular beam epitaxy

ABSTRACT

Optical and structural properties of submonolayer InGaAs/GaAs quantum dot solar cells (SML-QDSCs) are investigated and compared with quantum well solar cells (QWSCs). Compared with InGaAs/GaAs QWSCs with a similar structure, the material quality for SML QDSCs is significantly improved with a reduced density of both crosshatch patterns and defects. This coincides with a much higher photoluminescence intensity obtained for SML QDSCs. SML QDSCs thus exhibit an increase in open circuit voltage of 70 meV and an improvement in short circuit current from 15.9 mA/cm^2 to 17.7 mA/cm^2 in comparison with QWSCs. These findings present a promising alternative to quantum wells in photovoltaic applications.

1. Introduction

The energy crisis and environmental issues require urgent development of renewable energies. Considerable attention has been paid to solar energy, which is abundant, inexhaustible, and clean [1]. To make solar energy more affordable and accessible to everyone, great efforts have been made on photovoltaic cells with low cost per Watt, which depends on the solar cell power conversion efficiency. Multijunction solar cells are promising in realizing the third generation solar cells with ultrahigh efficieny [2]. However, the lattice and current mismatch between subcells poses a major challenge to further improve the device efficiency. Lattice-matched subcells consisting of quantum structures have been proposed to obtain the optimal energy bandgap and current matching for multijunction solar cells [3,4]. The quantised energy levels in the semiconductor nanostructures, such as quantum wells (QWs) and quantum dots (QDs), can introduce additional absorption in the cell and provide a better way to manage the current matching [5–7] or to implement intermediate band solar cells [8–10].

Quantum well solar cells (QWSCs) made from III–V nanomaterials, such as InGaAs/GaAs QWs, have demonstrated improved short-circuit current density (J_{sc}) due to extended photon absorption compared with their bulk counterpart. However, the lattice mismatch between the InGaAs QW structures and the GaAs matrix materials places an upper limit on the number of InGaAs QWs that can be incorporated into the devices, and hence the contribution of sub-bandgap photon absorption to photocurrent remains marginal. As a result, strain-balanced InGaAs/GaAsP QWSCs have been developed as a means of overcoming the limits inherent to the strained approach [11]. Although it is possible to grow locally strained InGaAs/GaAsP layers which are unstrained with GaAs substrates, the strain at the InGaAs and GaAsP interface will limit the indium content and thickness of InGaAs QWs that is directly related to the absorption wavelength. Moreover, GaAsP strain-compensation layers will increase the barrier potential for the photo-generated carriers in InGaAs QWs, and hence reduce the escape rate of these carriers out of InGaAs QWs into base region. This is the key challenge for the further development of strain-balanced InGaAs/GaAsP QWSCs [12–14].

Submonolayer (SML) QDs are grown by depositing strained InAs with less than one monolayer coverage on the GaAs matrix. They have emerged as an alternative low-dimensional nanostructure to the conventional Stranski–Krastanov QDs and QWs. SML QDs possess several advantages, such as high areal density, high uniformity, absence of the wetting layer, and adjustable aspect ratio [15,16]. The dense and uniform SML QDs are promising in improving the sub-bandgap photon absorption. Despite these promising properties of SML QDs, photovoltaic cells made from such nanomaterials have not been studied [17]. In this letter, we report on the solar cells with incorporating multi-stacked InGaAs/GaAs SML QDs. The SML QDSCs are investigated in terms of the structural quality, optical properties, current–voltage characteristics, and quantum efficiency. A direct comparison is performed

* Corresponding author.
E-mail address: jiang.wu@ucl.ac.uk (J. Wu).

http://dx.doi.org/10.1016/j.solmat.2014.03.046

between SML QDSCs and InGaAs/GaAs QWSCs that have the same quantity of indium as the SML QDSCs. Compared with QWSCs, SML QDSCs have been demonstrated with better structural quality as well as optical property, because of the strain relaxation through formation of SML QDs. As a result, SML QDSCs show better J_{sc} and open circuit voltage (V_{oc}) than QWSCs.

Three samples, InGaAs/GaAs SML QDSC, InGaAs QWSC, and GaAs reference cell, were grown via a solid-source molecular beam epitaxy (MBE) on n-type GaAs (100) substrates. All solar cells have a similar p–i–n structure that consists of a 200 nm highly doped n-type GaAs buffer layer, 1000 nm n-type GaAs base, 420 nm intrinsic region, 250 nm p-type GaAs emitter, 30 nm p-type $Al_{0.75}Ga_{0.25}As$ window layer, and 50 nm highly doped p-type GaAs contact layer, as schematically shown in Fig. 1. SML QDs, QWs, and GaAs bulk material were grown in the intrinsic region for SML QDSC, QWSC, and GaAs reference cell, respectively. The intrinsic region of SML QDSC had 20 periods of stacked SML QD layers each separated by a 16 nm GaAs barrier. The stacked SML QD layers consisted of six alternating layers of 0.5 ML InAs and 2.5 ML GaAs. In the case of the QWSC, the stacked InAs/GaAs layers in SML QDSC were replaced by one 18 ML thick $In_{0.167}Ga_{0.833}As$ layer. High-growth-temperature GaAs spacer layers were used to suppress the formation of threading dislocations [18,19]. The surface morphology of the solar cell samples was characterised by a Veeco Nanoscope V atomic force microscope (AFM). Photoluminescence (PL) spectra of the samples were recorded by a Peltier cooled Ge detector under excitation from a 532 nm diode-pumped solid-state laser. The excitation power was fixed at 30 mW. Ohmic contacts were made by evaporating Au/Zn/Au and Ni/AuGe/Ni/Au for the p and n contacts, respectively. No anti-reflection coating was applied on the solar cell surfaces. The current density versus voltage (J–V) characteristics of the solar cells were measured under 1 sun AM 1.5G illumination at 25 °C. The external quantum efficiency (EQE) was measured at room temperature and zero bias.

Fig. 2 shows the AFM images for the surfaces of InAs/GaAs SML QDSC and the reference InGaAs/GaAs QWSC. The crosshatch patterns aligned along [011] and [0 − 11] directions are observed on the surfaces of SML QDSC and QWSC. The formation of crosshatch patterns often appears for lattice-mismatched hetero-epitaxy, but the origin of their formation remains controversial. Strain-relaxation is reported to introduce surface undulation and/or local enhancement of growth rate over the misfit dislocations, which is the primary cause attributed to the creation of crosshatch patterns [20]. As an equal amount of indium was supplied to the SML QDSC and QWSC, the same degree of surface undulation should be expected. Interestingly, the QWSC clearly appears to have a rougher surface with a higher density of ridges. Fig. 2(c) shows the AFM line profiles along the two orthogonal ⟨011⟩ directions on both cell surfaces. The profile roughness along [0 − 11] is 0.45 nm and 0.54 nm for SML QDSC and QWSC, respectively. However, the profile roughness along [011] is 0.24 nm and 0.39 nm for SML QDSC and QWSC, respectively. The difference of surface roughness in orthogonal ⟨011⟩ directions is attributed to the anisotropic strain relaxation in the two directions [21]. The difference between the crosshatch patterns on both surfaces indicates that the strain relaxation is different during the hetero-epitaxy growth of SML QDSC and QWSC. While depositing fractional coverage of InAs, indium segregation leads to InAs agglomerations that cause three-dimensional shape transformation or compositional modulation. At high indium concentration, three-dimensional islands tend to nucleate and result in QD potential wells. However, for dilute indium concentration QD potential well formation is mainly attributed to the presence of localised InAs rich regions [22]. This is in agreement with transmission electron microscopy (TEM) images shown in Fig. 3, in which the low indium concentration was observed for both SML QDs and QWs. The formation of InAs agglomerations will partially compensate the lattice-mismatch between InAs and GaAs. The undulated surface formed by elastic strain-relaxation is thus less prominent for the SML QDSC. The accumulation of strain in the multilayer QWs not only leads to the rougher surface, but also results in the defect formation directly below the multiple QWs to relax the strain as shown in the TEM image Fig. 3(a). In comparison, there is no defect observed for the SML QDSC shown in Fig. 3(b).

The PL spectra of the QWSC and the SML QDSC are compared in Fig. 4. At room temperature, both SCs show a narrow emission peaked at ~960 nm. The full-width at half-maximum of the PL spectrum is 11.6 nm and 12.6 nm for the QWSC and the SML QDSC, respectively. SML QD is confirmed to be a mixed quantum well-dot structure and the submonolayer deposition of InAs in GaAs matrix forms InAs rich two-dimensional islands in InGaAs wells [22,23]. As a result, SML QDs show similar shallow confinement as QWs. Despite the similarity in spectrum shape, the PL intensity of SML QDSC is significantly higher than that of the QWSC. This could be explained in terms of the misfit dislocations generated in QWSCs as observed in Fig. 3(a). These misfit dislocations can act as non-radiative recombination centres that will dramatically reduce the PL. In order to obtain further insight into the optical properties of the SCs, temperature-dependent PL measurements were carried out and the integrated PL intensities are plotted as a function of temperature in Fig. 4(b). The SML QDSC exhibits stronger emission compared to the QWSC over the full range of temperatures, which confirms improved optical properties of the SML QDSCs. The Arrhenius equation is used to fit the temperature-dependent integrated PL data. Thermal activation energies obtained from

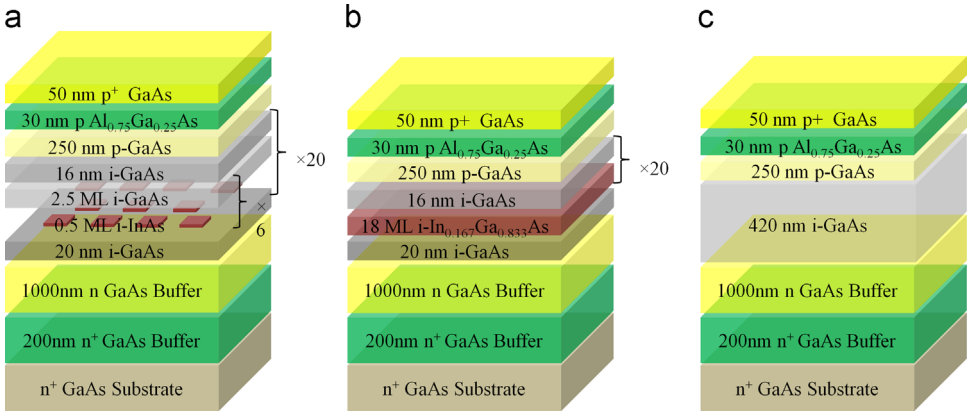

Fig. 1. Schematics of the (a) SML QDSC, (b) QWSC, and (c) GaAs reference solar cell structures.

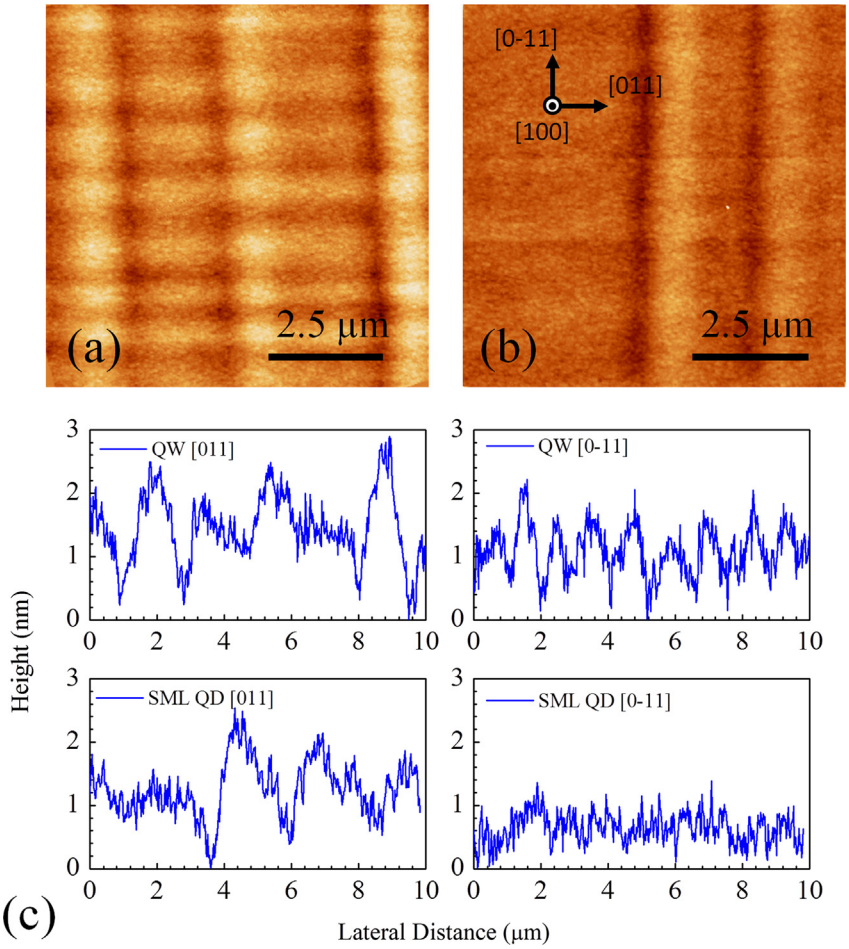

Fig. 2. Atomic force microscopy images of the surface morphology of (a) quantum well solar cell (QWSC) and (b) sub-monolayer quantum dot solar cell (SML QDSC). The *z*-scale is 5 nm for both images. (c) AFM line profiles along [011] direction (left) and [0−11] direction (right) on the QWSC surface (top) and SML QDSC (bottom).

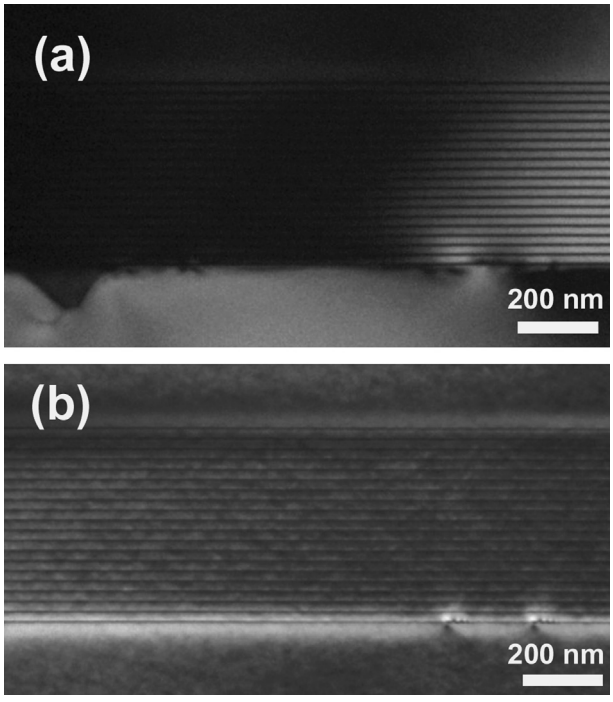

Fig. 3. Dark field (200) cross-sectional transmission electron microscopy images of InGaAs/GaAs (a) quantum wells in a quantum well solar cell and (b) multilayer sub-monolayer quantum dots in a quantum dot solar cell.

the Arrhenius fitting are 58 meV and 64 meV for the SML QDSC and QWSC, respectively. The slightly higher thermal activation energy for the SML QDSC suggests three-dimensional confinement in InAs rich regions leads to stronger quantum confinement. This enhancement of quantum confinement is also reflected in the PL spectra in Fig. 4(a), which shows the blueshift of PL peak for the SML QDSC compared to the QWSC.

Fig. 5(a) shows the EQE spectra of the SML QDSC, QWSC, and GaAs reference cell. Compared to the GaAs reference cell, the additional spectral response at ~960 nm is observed for both SML QDSC and QWSC. The EQE below the GaAs bandgap (~10%) is comparable to the sub-bandgap EQE of Stranski–Krastanov QDSC that originates from wetting layer absorption; but it is distinctly higher than that measured from QDs (typically 1%) [24,25]. Both the EQEs of the SML QDSC and QWSC above GaAs bandgap (< 870 nm) are reduced compared to the GaAs reference cell. This EQE reduction can be attributed to the reduced carrier lifetime due to formation of defects caused by strain, such as crosshatches observed in Fig. 2. In addition, the EQE of the QWSC with energies above GaAs bandgap is lower than that of the SML QDSC. AFM, TEM and PL measurements have demonstrated the improved crystal quality of the SML QDSC, as a result of strain-relaxation caused by the formation of InAs agglomerations and the suppression of defect formation. Compared to the SML QDSC, the formation of dislocations in the QWSC will increase non-radiative recombination, which will reduce the collection efficiency of photo-generated carriers, and hence degrade the EQE. The *J*–*V* characteristics under 1 sun AM1.5G illumination are shown in

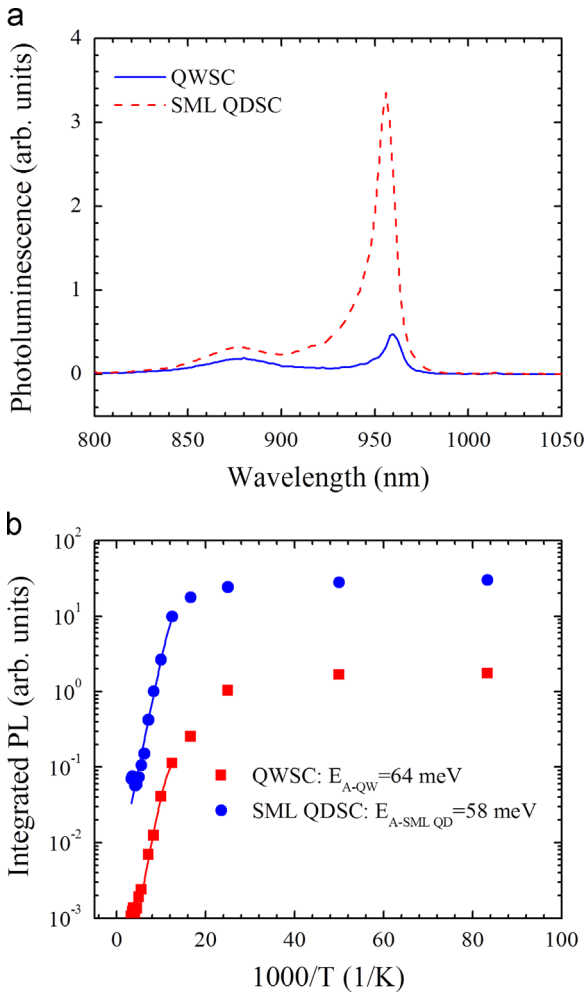

Fig. 4. (a) Photoluminescence (PL) spectra of the SML QDSC and QWSC at room temperature. (b) Temperature-dependent integrated PL intensities of SML QDSC and QWSC. Arrhenius fitting results are shown for SML QDSC and QWSC.

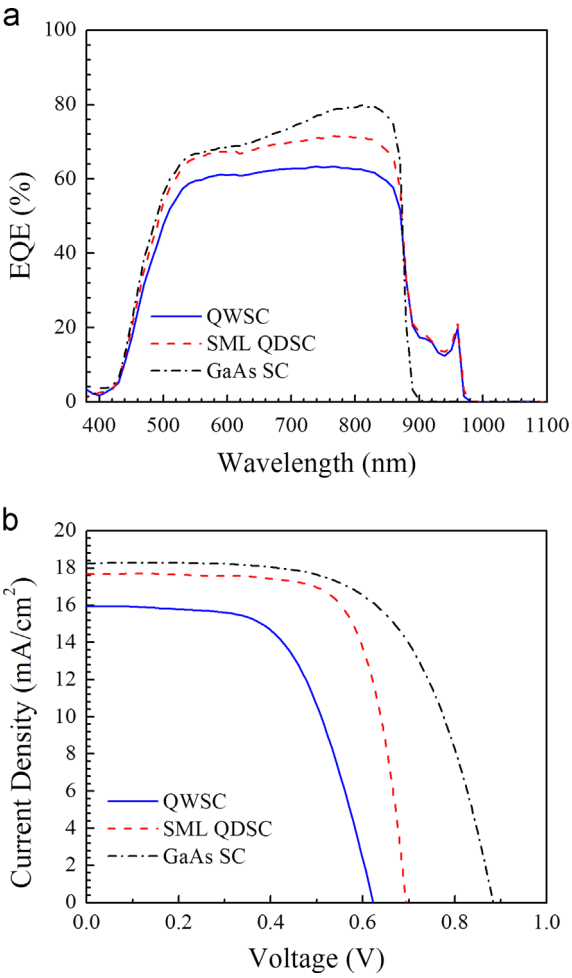

Fig. 5. (a) External quantum efficiency curves and (b) current density versus voltage characteristics under 1 sun AM 1.5G illumination for the SML QDSC, QWSC, and GaAs reference solar cell.

Fig. 5(b). In agreement with the EQE measurements, both the SML QDSC and QWCS shows lower quantum efficiency than that of the GaAs reference cell which has the highest J_{sc} of 18.2 mA/cm^2. However, the improved material quality has enabled the SML QDSC to obtain a recovered J_{sc} of 17.7 mA/cm^2, compared to 15.9 mA/cm^2 for the QWSC. The V_{oc} of the SML QDSC is 0.69 V, which is slightly higher than 0.62 V obtained for the QWSC. Since the effective bandgap is about the same for SML QDSC and QWSC, the reduction in V_{oc} for QWSC could be well explained by the formation of dislocations, as observed in Fig. 3(a). The SML QDSC shows a higher efficiency of 7.0% than that of 4.7% for the QWSC. Here it should be noted that, the material quality of InGaAs QWSCs and SML QDSCs could be significantly enhanced by using a GaAsP strain-compensation layer, and hence the performance of InGaAs QWSCs and SML QDSCs. However, the GaAsP compensation layer will increase the potential barrier, and hence suppress the escape rate of photo-generated carriers out of InGaAs QWs. For InGaAs SML QDSCs, a GaAsP strain-compensation layer with less phosphorus content is required to ensure the material quality. Therefore, a higher escape rate of photo-generated carriers is expected for InGaAs SML QDSCs compared to InGaAs QWSCs, which consequently results in higher J_{sc}.

In summary, the InGaAs/GaAs SML QDSC is proposed and demonstrated in this work. The material quality and device performance of the SML QDSCs are compared with those of InGaAs/GaAs QWSCs. By replacing the QWs with SML QDs, both the structural and optical properties of the solar cells have been improved, because of the unique strain relaxation mechanism of SML QDs. In comparison with QWSCs, the SML QDSCs show an enhanced V_{oc} from 0.62 V to 0.69 V and increased J_{sc} from 15.9 mA/cm^2 to 17.7 mA/cm^2. By using the strain-balancing technique, further improvements in J_{sc} and V_{oc} for SML QDSCs are expected. SML QDs thus show promise as an alternative to QWs in the implementation of high-efficient solar cells.

Acknowledgements

The authors acknowledge the financial support of EPSRC Grant EP/K029118/1. H. Liu would like to thank The Royal Society for funding his University Research Fellowship.

References

[1] S. Ito, S.M. Zakeeruddin, P. Comte, P. Liska, D Kuang, M. Grätzel, Nat. Photonics 2 (2008) 693.
[2] R.R. King, D.C. Law, K.M. Edmondson, C.M. Fetzer, G.S. Kinsey, H. Yoon, R.A. Sherif, N.H. Karam, Appl. Phys. Lett. 90 (2007) 183516.
[3] P. Kailuweit, R. Kellenbenz, SP Philipps, W. Guter, AW Bett, F. Dimroth, J. Appl. Phys. 107 (2010) 064317.
[4] C. E. Valdivia, S. Chow, S. Fafard, O. Thériault, M. Yandt, J. F. Wheeldon, A. J. SpringThorpe, B. Rioux, D. McMeekin and D. Masson, in: Proceedings of the IEEE 35th Photovoltaics Specialist Conference, 2010, p. 001253.

[5] S.M. Hubbard, C.D. Cress, C.G. Bailey, R.P. Raffaelle, S.G. Bailey, D.M. Wilt, Appl. Phys. Lett. 92 (2008) 123512.
[6] J. Wu, Y.F. Makableh, R. Vasan, M.O. Manasreh, B. Liang, C.J. Reyner, D.L. Huffaker, Appl. Phys. Lett. 100 (2012) 051907.
[7] K.H. Lee, K.W. Barnham, J.P. Connolly, B.C. Browne, R.J. Airey, J.S. Roberts, M. Fuhrer, T.N. Tibbits, N.J. Ekins-Daukes, IEEE J. Photovolt. 2 (2012) 68–74.
[8] A. Martí, E. Antolín, C.R. Stanley, C.D. Farmer, N. López, P. Díaz, E. Cánovas, P.G. Linares, A. Luque, Phys. Rev. Lett. 97 (2006) 247701.
[9] Y. Okada, T. Morioka, K. Yoshida, R. Oshima, Y. Shoji, T. Inoue, T. Kita, J. Appl. Phys. 109 (2011) 024301.
[10] A. Luque, A. Marti, Adv. Mater. 22 (2010) 160.
[11] J.G. J. Adams, B.C. Browne, I.M. Ballard, J.P. Connolly, N.L. A. Chan, A. Ioannides, W. Elder, P.N. Stavrinou, K.W. J. Barnham, N.J. Ekins-Daukes, Prog. Photovolt. 19 (2011) 865–877.
[12] Y. Okada, N. Shiotsuka, T. Takeda, Sol. Energy Mater. Sol. Cells 85 (2005) 143–152.
[13] J. Mohaidat, K. Shum, W. Wang, R. Alfanoasb, J. Appl. Phys. 76 (1994) 5533.
[14] Y. Wen, Y. Wang, K. Watanabe, M. Sugiyama, Y. Nakano, IEEE J. Photovolt. 3 (2013) 289–294.
[15] Z. Xu, D. Birkedal, M. Juhl, J.M. Hvam, Appl. Phys. Lett. 85 (2004) 3259.
[16] J.O. Kim, S. Sengupta, Y. Sharma, A.V. Barve, S.J. Lee, S. Krishna, S. K Noh, Proc. SPIE 8353 (2012) 835336.
[17] J.O. Kim, S. Sengupta, A.V. Barve, Y.D. Sharma, S. Adhikary, S.J. Lee, S.K. Noh, M.S. Allen, J.W. Allen, S. Chakrabarti, Appl. Phys. Lett. 102 (2013) 011131.
[18] F.K. Tutu, I.R. Sellers, M.G. Peinado, C.E. Pastore, S.M. Willis, A.R. Watt, T. Wang, H.Y. Liu, J. Appl. Phys. 111 (2012) 046101.
[19] H.Y. Liu, I.R. Sellers, T.J. Badcock, D.J. Mowbray, M.S. Skolnick, K.M. Groom, M. Gutierrez, M. Hopkinson, J.S. Ng, J.P. R. David, Appl. Phys. Lett. 85 (2004) 704.
[20] S. Saha, D.T. Cassidy, D.A. Thompson, J. Appl. Phys. 113 (2013) 124301.
[21] O. Yastrubchak, T. Wosiński, JZ Domagała, E. Łusakowska, T. Figielski, B. Pecz, AL Toth, J. Phys.: Condens. Matter 16 (2004) S1.
[22] F. Hopfer, A. Mutig, M. Kuntz, G. Fiol, D. Bimberg, NN Ledentsov, VA Shchukin, SS Mikhrin, DL Livshits, IL Krestnikov, Appl. Phys. Lett. 89 (2006) 141106.
[23] Z. Xu, K. Leosson, D. Birkedal, V. Lyssenko, J.M. Hvam, J. Sadowski, Nanotechnology 14 (2003) 1259–1261.
[24] Phu Lam Frank Tutu, Jiang Wu, Naoya Miyashita, Yoshitaka Okada, Kan-Hua Lee, Nicholas Ekins-Daukes, James Wilson, Huiyun Liu, Appl. Phys. Lett. 102 (2013) 163907.
[25] J. Wu, S.C. Mangham, V.R. Reddy, M.O. Manasreh, B.D. Weaver, Sol. Energy Mater. Sol. Cells 102 (2012) 44.